Linear Parameter Varying Control Synthesis for the atmospheric phase VEGA launcher ⋆

D. Navarro-Tapia * **A. Marcos** * **S. Bennani** ** **C. Roux** ***

* *Technology for Aerospace Control (TASC) Group, University of Bristol, Bristol, BS8 1TR, United Kingdom; (e-mail: diego.navarro-tapia/andres.marcos@bristol.ac.uk)*
** *ESA-ESTEC, Noordwijk, 2201AZ, The Netherlands; (e-mail: samir.bennani@esa.int)*
*** *ELV S.p.A., Colleferro, 00034, Italy; (e-mail: christophe.roux@elv.it)*

Abstract: This article presents the design of the atmospheric control system of a launch vehicle using the Linear Parameter Varying (LPV) synthesis technique. The main goal is to facilitate the transfer of this technique, already well known for providing a systematic design approach with reduced effort, to the European launcher industrial domain. In this paper, a grid-based LPV approach is applied to the actual VEGA VV05 mission data for the joint design of the rigid-body controller and the flexible bending filter in one single design procedure. The LPV controller is analysed in terms of classical linear stability margins and evaluated and compared with the VEGA baseline controller via Monte-Carlo analyses using a high-fidelity, nonlinear simulator. The results show that the LPV controller provides satisfactory stability margins and excellent performance and robustness characteristics while offering a more systematic and methodological design approach.

Keywords: aerospace control, robust control

1. INTRODUCTION

The design of the atmospheric-phase control system of a launch vehicle is a challenging control problem. The controller must be able to provide stabilisation and cope with different competing performance requirements in the face of a wide range of system variations, environmental perturbations and parameters dispersion. Furthermore, the bending modes caused by the elastic behaviour of the launch vehicle must be attenuated to ensure robust stability. The VEGA launcher uses a classical controller framework for the Thrust Vector Control (TVC) system (Roux and Cruciani, 2008), which has been proved to be successful in the eleven flights VEGA has performed so far. Nonetheless, the need of providing higher robustness/performance as well as reducing the control tuning effort and cost prior each flight has led to investigate the use of advanced and robust control techniques such as LPV control design.

The LPV framework can be considered as an augmentation of the standard $\mathcal{H}_\infty$ approach, which is based on Linear Time Invariant (LTI) models. A LPV model captures the time-varying behaviour of the system based on a defined scheduling parameter. This information is used by the LPV design process to generate in a single step a scheduled controller on the chosen parameter.

⋆ This work is funded by ESA through the Networking/Partnering Initiative contract No. 4000114460/15/NL/MH/ats. Mr. Navarro-Tapia is also the recipient of a Doctoral Training Partnership award No. 1609551 by the UK Engineering and Physical Sciences Research Council (EPSRC).

This approach has been applied to numerous works in aerospace applications (Balas, 2002; Marcos and Balas, 2004; Marcos and Bennani, 2009, 2011) and also including launch vehicle control design (Ganet and Ducamp, 2010).

This article extends the work done in reference (Navarro-Tapia et al., 2017), where a rigid-body non-rate bounded LPV design was performed. In this case, a rate bounded design is considered and the flexible-body dynamics of the launch vehicle are also included. Traditionally, the design of the rigid-body controller and bending filters are addressed separately in an iterative fashion. As for the bending filter design, different design approaches can be found in the literature. For example, in reference Brito et al. (2008) a Recursive Least Squares (RLS) method is used to estimate the most suitable configuration for a notch filter. Also, in references Orr (2013) and Bedrossian et al. (2005) the bending filter design is formulated as a constrained numerical optimization.

In this paper, the design of the rigid-body controller and bending filters is unified in the same design process. By proper choice of the frequency-domain design weighting functions, the LPV synthesis approach can generate a LPV controller, which performs rigid-body control and bending stabilization.

The layout of the article is as follows: Section 2 describes the LPV modeling approach for the VEGA launch vehicle. Section 3 is dedicated to the LPV control synthesis formulation. Finally, the LPV design is analysed and validated through Monte-Carlo nonlinear simulations. Finally, conclusions are given in Section 5.

2. VEGA LAUNCH VEHICLE

VEGA launcher is the new European Small Launch Vehicle developed under the responsibility of the European Space Agency (ESA) and European Launch Vehicle (ELV S.p.A.) as prime contractor. The launcher has successfully performed eleven launches since its maiden flight on 13^{th} February 2012.

VEGA is a single-body launcher, which follows a four-stage approach. All stages are controlled using a TVC system and a roll and attitude control system (RACS) during the propelled phases.

2.1 VEGA launcher model

The VEGA launcher model is described by the standard six-degree-of-freedom equations of motion, which account for the translational and rotational dynamics of the launch vehicle. Due to axial symmetry of the vehicle about the roll axis and assuming a low roll rate, the pitch and yaw axes can be considered uncoupled and more importantly equal. In this work, the VEGA launch vehicle will be examined in the yaw plane (see Figure 1).

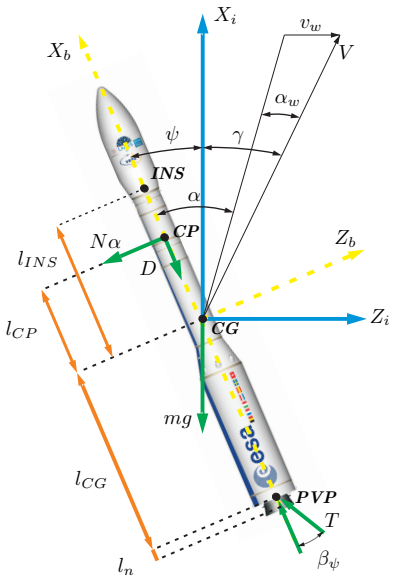

Fig. 1. VEGA yaw-motion diagram

The launch vehicle equations are expressed as the sum of forces and moments from rigid-body, flexible-body and nozzle dynamics.

$$m\ddot{z} = \Sigma F = F_r + F_f + F_n \tag{1}$$

$$J_{yy}\ddot{\psi} = \Sigma M = M_r + M_f + M_n \tag{2}$$

with m is the vehicle mass, J_{yy} is the lateral moment of inertia, $\ddot{z}$ is the linear drift acceleration and $\ddot{\psi}$ the yaw attitude acceleration.

The reader is referred to Navarro-Tapia et al. (2017) for further details on the derivation of the rigid-body and nozzle equations. As for the flexible-body motion, the dynamics of the i^{th} bending mode are represented by a 2^{nd} order model with a natural frequency ω_{q_i} and a low damping ratio ζ_{q_i}.

All relevant dynamics are represented using the state-space formulation shown in equation 3, where the rigid- and flexible-body contributions are expressed separately. The matrices of this state-space model are given in equation 4. The model uses four rigid-body states given by the drift z, yaw attitude angle ψ and their derivatives ($\mathbf{x_r} = \begin{bmatrix} z & \dot{z} & \psi & \dot{\psi} \end{bmatrix}^T$); two flexible-body states accounting for one flexible mode ($\mathbf{x_f} = \begin{bmatrix} q_1 & \dot{q_1} \end{bmatrix}^T$); three inputs ($\mathbf{u_{LV}} = \begin{bmatrix} \beta_\psi & \ddot{\beta}_\psi & v_w \end{bmatrix}^T$), with β_ψ the nozzle deflection angle and v_w the wind velocity; and five outputs ($\mathbf{y_{LV}} = \begin{bmatrix} Q\alpha & \psi_{INS} & \dot{\psi}_{INS} & z_{INS} & \dot{z}_{INS} \end{bmatrix}^T$), which include the load performance indicator $Q\alpha$ (with Q the dynamic pressure and α the angle of attack), and the inertial navigation system (INS) measurements at node location for the four states.

$$\begin{bmatrix} \dot{\mathbf{x}}_\mathbf{r} \\ \dot{\mathbf{x}}_\mathbf{f} \end{bmatrix} = \begin{bmatrix} A_r & A_{rf} \\ A_{fr} & A_f \end{bmatrix} \begin{bmatrix} \mathbf{x_r} \\ \mathbf{x_f} \end{bmatrix} + \begin{bmatrix} B_r \\ B_f \end{bmatrix} \mathbf{u_{LV}}$$

$$\mathbf{y_{LV}} = \begin{bmatrix} C_r & C_f \end{bmatrix} \begin{bmatrix} \mathbf{x_r} \\ \mathbf{x_f} \end{bmatrix} + D\mathbf{u_{LV}} \tag{3}$$

$$A = \left[\begin{array}{cccc:cc} 0 & 1 & 0 & 0 & 0 & 0 \\ 0 & a_1 & a_3 & a_2 & a_{zq} & 0 \\ 0 & 0 & 0 & 1 & 0 & 0 \\ 0 & a_4 & a_6 & a_5 & a_{\psi q} & 0 \\ \hdashline 0 & 0 & 0 & 0 & 0 & 1 \\ 0 & 0 & 0 & 0 & a_{qq} & a_{q\dot{q}} \end{array}\right] \quad B = \left[\begin{array}{ccc} 0 & 0 & 0 \\ a_p & k_2 & -a_1 \\ 0 & 0 & 0 \\ k_1 & k_3 & -a_4 \\ \hdashline 0 & 0 & 0 \\ a_{q\beta} & a_{q\ddot{\beta}} & 0 \end{array}\right] \tag{4}$$

$$C = \left[\begin{array}{cccc:cc} 0 & \frac{Q}{V} & Q & 0 & 0 & 0 \\ 0 & 0 & 1 & 0 & -\Psi'_{INS1} & 0 \\ 0 & 0 & 0 & 1 & 0 & -\Psi'_{INS1} \\ 1 & 0 & -l_{INS} & 0 & \Psi_{INS1} & 0 \\ 0 & 1 & 0 & -l_{INS} & 0 & \Psi_{INS1} \end{array}\right] D = \left[\begin{array}{ccc} 0 & 0 & \frac{-Q}{V} \\ 0 & 0 & 0 \\ 0 & 0 & 0 \\ 0 & 0 & 0 \\ 0 & 0 & 0 \end{array}\right]$$

with V the vehicle velocity and l_{INS} the distance from the center of gravity (CG) to INS. Finally, Ψ_{INS1} and Ψ'_{INS1} are the rotational and translational lengths of the first bending mode at INS respectively.

The rigid-body matrix coefficients can be found in reference Navarro-Tapia et al. (2017). The flexible-body coefficients are given by:

$$\begin{aligned} a_{zq} &= \tfrac{T}{m}\Psi'_{PVP1}; \quad & a_{\psi q} &= \tfrac{T}{J_{yy}}(\Psi'_{PVP1} l_{CG} + \Psi_{PVP1}); \\ a_{q\beta} &= -T\Psi_{PVP1}; \quad & a_{q\ddot{\beta}} &= \mathrm{I_n}\Psi'_{PVP1} - m_n l_n \Psi_{PVP1}; \\ a_{qq} &= -\omega_{q1}^2; \quad & a_{q\dot{q}} &= -2\zeta_{q1}\omega_{q1}; \end{aligned} \tag{5}$$

where T is the thrust force, l_{CG} the distance from CG to the nozzle pivot point (PVP), m_n the nozzle engine mass, $\mathrm{I_n}$ the moment of inertia of the nozzle about PVP and l_n the distance from the nozzle CG to PVP. Numerical values for the coefficients are not given due to confidentiality reasons.

2.2 LPV modelling

In order to support the LPV control design, first an LPV model of VEGA launcher is formulated by expressing the system as a function of a set of time-varying scheduling parameters $\theta(t)$ as shown in equation 6.

$$\dot{x}(t) = A[\theta(t)]x(t) + B[\theta(t)]u_{LV}(t)$$
$$y_{LV}(t) = C[\theta(t)]x(t) + D[\theta(t)]u_{LV}(t) \quad (6)$$

The values of $\theta(t)$ are defined within a region Ω and have a known bound on the rate variation $\underline{v} \leq \dot{\theta} \leq \overline{v}$. In addition, note that the time variation of $\theta(t)$ is assumed to be unknown but measurable in real time.

In this work, the VEGA LPV model is built using the recently developed MATLAB toolbox LPVTools (Hjartarson et al., 2015). In particular, a grid-based approach is employed using a set of 6 linearised plants throughout the atmospheric phase (at t = [20 40 50 60 70 90]s). The time-varying parameter used to build the LPV model is the non-gravitational velocity (θ = VNG), which is the one implemented in VEGA for gain scheduling purposes (Roux and Cruciani, 2008). Figure 2 shows the time evolution of VNG and its rate, the non-gravitational acceleration (ANG), for the VEGA VV05 mission. Therefore, in this case, the region Ω is defined by 6 points within the range $\theta = [433 - 2345]$ m/s with rate bound $17 < \dot{\theta} < 40$ m/s^2.

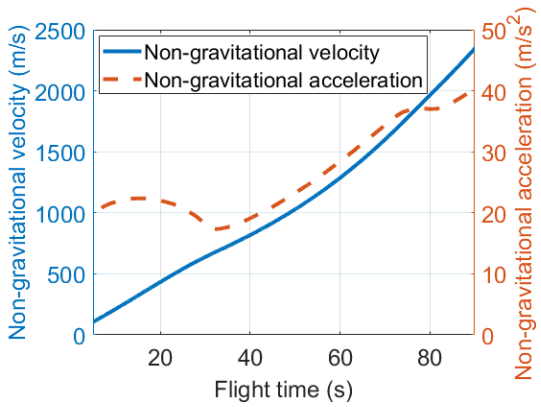

Fig. 2. Non-gravitational velocity and acceleration for VEGA VV05 flight

At each grid point, the LPV model is described by the respective LTI model at that point. However, at flight instants between the grid points, the LPV system is linearly interpolated. In order to ensure that the LPV model captures the main launcher dynamics, the frequency responses of the LPV model (frozen at specific scheduling variable instances) and the corresponding LTI models at those instances are compared. This validation process can be seen in Navarro-Tapia et al. (2017), where the LPV model validation is illustrated with two different flight instants.

3. LINEAR PARAMETER VARYING SYNTHESIS

This section describes the design of the VEGA atmospheric phase control system using the LPV synthesis technique.

3.1 Problem formulation

The control design problem is formulated as the generalized plant interconnection shown in Figure 3 (shown in the next page for clarity), where the main input-output channels of the closed-loop system are scaled by frequency-domain weighting functions represented by shaded blocks. These weighting functions are shaped to specify the control design objectives and its selection will be discussed in Section 3.2.

The closed-loop interconnection is composed of 5 main blocks: $K(s,\theta)$ is the LPV controller; $G_{LV}(s,\theta)$ is the VEGA LPV model; $G_{TVC}(s)$ and $G_\tau(s)$ represent the actuator dynamics and the delays originated by the on-board computers and actuators (more details about these two models can be found in reference Simplício et al. (2016)); and finally, $G_w(s,\theta)$ is a LPV wind turbulence model that is included in the design process to improve the wind disturbance rejection performance. This block is described in detail in reference Navarro-Tapia et al. (2017).

The generalised plant interconnection can also be expressed as a standard $\mathcal{H}_\infty$ formulation (see Figure 4), where the closed-loop system is merged into a LPV generalized plant $P(s,\theta)$ which gathers commands, wind disturbance and sensor noise inputs as exogenous inputs ($\mathbf{d} = \left[\mathbf{d_c}^T \; d_w \; \mathbf{d_n}^T\right]^T$) and error and performance variables as exogenous outputs ($\mathbf{e} = \left[e_{\psi_e} \; \mathbf{e_{INS}}^T \; e_{Q\alpha} \; e_u\right]^T$). The controller output and inputs are represented by u and the vector $\mathbf{y} = \left[\psi_e \; \dot{\psi}_e \; z_e \; \dot{z}_e\right]^T$. Finally, vectors $\mathbf{e}$ and $\mathbf{d}$ are scaled by the weighting functions forming the augmented generalised plant $\tilde{P}(s,\theta)$.

The LPV synthesis optimisation consists of finding the controller $K(s,\theta)$ which minimises the induced $\mathcal{L}_2$ norm of the cost function in equation 7 for all allowable time-varying parameter trajectories. For a LTI plant, the induced $\mathcal{L}_2$ norm is equivalent to the $\mathcal{H}_\infty$ norm.

$$\min_{K(s,\theta)} ||\mathcal{F}_l(\tilde{P}(s,\theta), K(s,\theta))||_{\mathcal{L}_2} \quad \text{for} \quad \begin{matrix} \theta \in \Omega \\ 17 < \dot{\theta} < 40 \text{ m/s}^2 \end{matrix} \quad (7)$$

where $\mathcal{F}_l$ denotes the lower linear fractional transformation and represents the transfer function from $\mathbf{d}'$ to $\mathbf{e}'$.

The described LPV synthesis approach is also implemented in the LPVTools toolbox (Hjartarson et al., 2015) through the command *lpvsyn*.

3.2 Weighting function selection

Due to the wide dynamic variation of the mission, the design objectives change along the atmospheric phase. To cope with that, for each grid point a different set of weighting functions is defined. And then, LPV models of the weights W_{in} and W_{out} are obtained using the same grid-based approach used for the VEGA LPV modelling.

The design uses the weight setup rationale from reference Navarro-Tapia et al. (2017). Next, the weighting functions are briefly described. At the input side, W_c is composed of constants which are defined to balance the command channels. W_w represents the standard deviation of the unitary white noise n_w input for the wind disturbance model $G_w(s,\theta)$ while W_n models the sensor noise of each feedback measurement.

At the output side, W_{INS} is a diagonal matrix which bounds the classical yaw attitude complementary sensitivity function ($T_\psi = \psi_{INS}/\psi_c$) and also specifies the lateral control requirements on the design process. W_{ψ_e} bounds the yaw sensitivity function ($S_\psi = \psi_e/\psi_c$) while $W_{Q\alpha}$ defines a constraint on the maximum α.

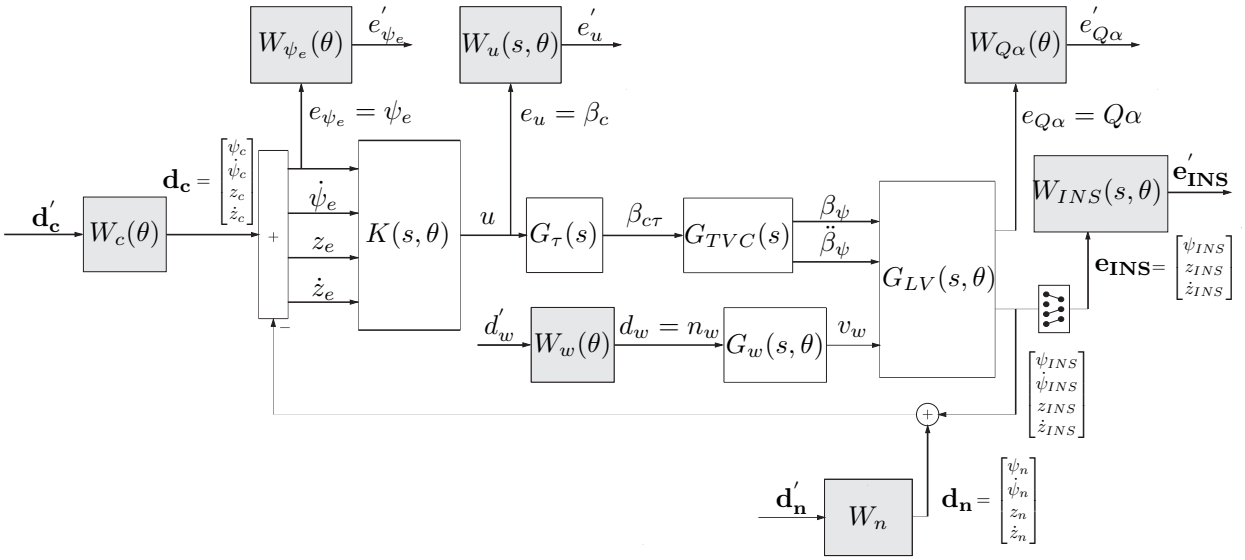

Fig. 3. Generalised plant interconnection for the VEGA LPV control design

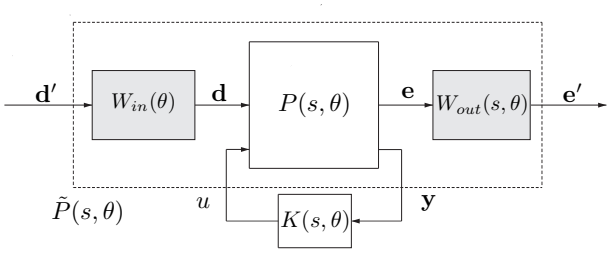

Fig. 4. Standard $\mathcal{H}_\infty$ interconnection

Finally, in order to attenuate the 1^{st} bending mode and also reduce the control effort at high frequencies, the control output u is weighted with the inverse of equation 8 (see also Figure 5). As it can be seen, W_u^{-1} is composed of two notch filters centered at the maximum and minimum expected dispersion of the 1^{st} bending mode frequency due to uncertainties ($\omega_{q_1} = [\underline{\omega_{q_1}}, \overline{\omega_{q_1}}]$), plus a second order low-pass filter $F(s,\theta)$, which imposes an actuation bound at low-frequencies and also provides an attenuation of -30dB at high frequencies for the upper bending modes. This double-notch filter configuration offers a good trade-off between attenuation and phase response. It provides the necessary design flexibility to attenuate the 1^{st} bending mode while not degrading so much the rigid-body margins with phase delay.

$$W_u^{-1}(s,\theta) = \underbrace{\frac{s^2+0.5s+(\underline{\omega_{q_1}}(\theta))^2}{s^2+70s+(\underline{\omega_{q_1}}(\theta))^2}}_{\text{Notch 1}} \underbrace{\frac{s^2+0.5s+(\overline{\omega_{q_1}}(\theta))^2}{s^2+70s+(\overline{\omega_{q_1}}(\theta))^2}}_{\text{Notch 2}} \underbrace{F(s,\theta)}_{\text{Low-pass filter}} \quad (8)$$

3.3 LPV design

As a first step towards the LPV design, a linear $\mathcal{H}_\infty$ design is performed at each grid point. The main goal of the design is to reduce the wind disturbance contribution in the system. In terms of performance, a load-relief control mode is employed about the maximum dynamic pressure region (t=40,50,60s). For the rest of the grid points, the design is focused on minimising the tracking error while trying to keep the lateral deviations bounded. The $\mathcal{H}_\infty$-norm obtained by these linear designs are in the range between 1.18 and 1.84.

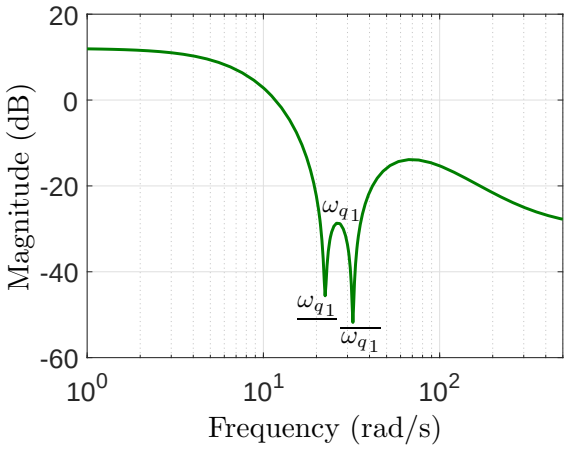

Fig. 5. Bode magnitude plot of $W_u^{-1}(s,\theta)$

Using the interconnection and weighting functions previously presented, a rate bounded LPV design is performed using VNG as time-varying parameter with the parameter grid described in Section 2.2.

The control problem is formulated as a linear matrix inequality (LMI) problem, which must be solved to generate a controller. The constraints on the rate variation of VNG are included via basis functions X_θ and Y_θ. This design is performed using quadratic basis functions such as $X_\theta = X_0 + X_1\theta + X_2\theta^2$ and $Y_\theta = Y_0 + Y_1\theta + Y_2\theta^2$. This configuration yields a good compromise between performance and complexity. For example, constant and linear dependent basis functions provide very poor performance, but more complex basis functions result in a very costly computational process, also due to the high order of the design plant.

Like the classical $\mathcal{H}_\infty$ control design approach, the applied LPV synthesis does not allow defining a specific controller structure and the resulting controller has as many states as those used in the design interconnection, which results in a 22^{th} order controller. The induced $\mathcal{L}_2$ norm of the LPV controller is 2.13 (which is only a 15% increase with respect to the highest linear $\mathcal{H}_\infty$ design norm).

4. SIMULATIONS

This section analyses first the LPV design in terms of the classical linear stability margins. Then, the LPV controller is compared with the VEGA baseline controller using ELV's nonlinear, high-fidelity benchmark with a Monte-Carlo campaign. It is highlighted that this campaign is not as intensive as that underwent by the baseline in the actual verification and validation (V&V) campaign prior to deployment and launch. Nonetheless, this comparison provides a fair and reliable assessment on the capability to improve the design using more methodological tools and methods.

4.1 Linear analysis

The stability margins are assessed in the frequency domain through Nichols plots. To that end, the open-loop system (controller, actuator and launch vehicle model) is re-arranged and broken at the controller output in order to reduce the system to a single-input single-output system.

Figure 6 shows the Nichols chart of the closed-loop system at distinct flight instants. To perform this analysis, a LTI controller is extracted from the LPV controller by interpolating at every 10 seconds in the range t=[20,90]s. Note that the rate of change of θ is fixed to the corresponding value of ANG at each flight instant (see Figure 2). Looking at Figure 6, it can be seen the LPV design provides satisfactory rigid-body margins while it yields gain stabilisation for the first and upper bending modes.

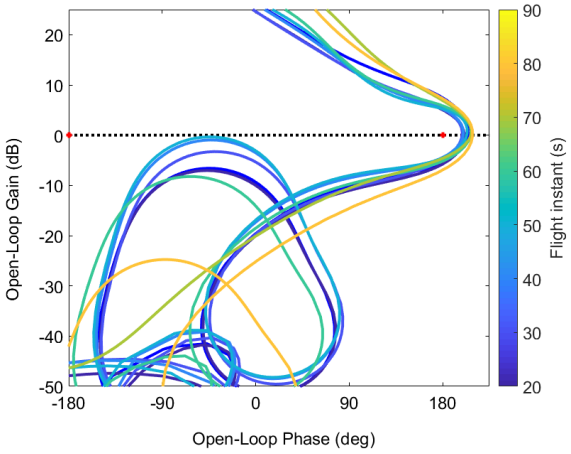

Fig. 6. Nichols charts for LPV design at $\dot{\theta}(t) = ANG(t)$

The stability margins are also evaluated at the minimum and maximum rate of change ($\dot{\theta}$ = 17,40 m/s^2). It is observed that the variation of the margins are less than 1% with respect to the case $\dot{\theta}(t) = ANG(t)$, except at $t = 20s$ and $t = 90s$, where the differences are below 5%.

4.2 Nonlinear analysis

Finally, the LPV design is implemented and validated in VEGACONTROL, which is a nonlinear 6 degrees-of-freedom high-fidelity simulator tailored to simulate the atmospheric phase for the VEGA launcher. This simulator allows to scatter more than 125 different operational parameters by means of normalised flags within the range [-1,1], being the zero value the nominal condition.

To evaluate the performance and robustness, four Monte-Carlo (MC) campaigns of 500 runs are performed (the same four MC set-ups are applied to the LPV design and the baseline controller used for the VEGA VV05 mission). For each run, the same nominal VEGA VV05 flight trajectory is used but the operational parameters are all dispersed randomly. Each of the four MC campaign uses the same scattering flags but a different wind profile (among them, the estimated wind encountered in VEGA VV05 mission). Note that the four wind profiles have been extracted from real measurements and cover strong and moderate wind gusts at different altitudes.

The baseline controller is implemented using the full VEGA TVC control architecture shown in reference Roux and Cruciani (2008), which comprises the rigid-body gains plus a set of H filters with different purposes. Differently, the VEGA LPV control structure is only composed of the LPV controller, which is implemented using a Simulink block provided in the LPVTools toolbox (Hjartarson et al., 2015) and a derivative filter H_2 to compute the attitude error rate signal. For the LPV simulation, a simpler H_2 filter based on a first order pseudo-derivative configuration has been synthesized, discretized and implemented.

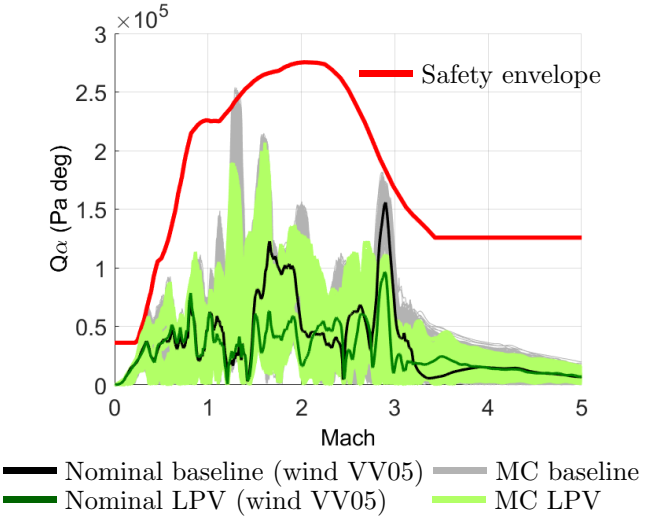

Fig. 7. VEGACONTROL MC $Q\alpha$ analysis

Figure 7 shows the 2000 (=4*500) MC responses for the aerodynamic load performance indicator $Q\alpha$ versus Mach for the baseline controller (left plot) and the LPV design (right plot). In darker lines, the corresponding simulations using the VEGA VV05 mission estimated wind and nominal dispersions are depicted for each controller to serve as reference.

Comparing both plots, it can be seen that the LPV controller reduces significantly the aerodynamic loads with respect to the baseline $Q\alpha$ performance. It should be remarked that this is not only achieved on a unique wind, but using the four different wind profiles, which includes the real wind from the flown VEGA VV05 mission. It can also be observed that the baseline controller presents several cases that violate the $Q\alpha$ safety envelope (around Mach 1.25), while the LPV design manages to reduce this performance indicator for that Mach point and throughout the flight envelope.

In addition, a quantitative assessment of the robustness of both designs for a set of performance indicators (such as attitude error, drift, or aerodynamic load performance) is performed. For each MC run, two different metrics

are computed for each indicator: the ∞-norm, which is equivalent to the maximum value taken by the variable, and the 2-norm, which accounts for the energy of the assessed indicator. Figure 8 shows the average of those two norms normalised with respect to the baseline controller.

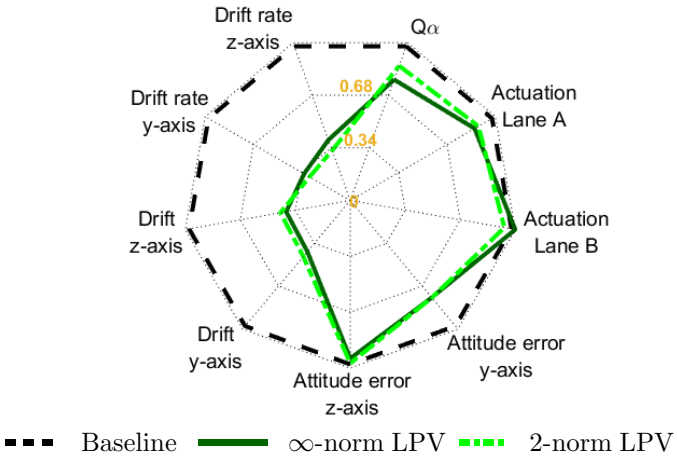

Fig. 8. MC analysis in terms of ∞-norm and 2-norm

Comparing the baseline and the LPV design, it can be seen that the latter offers improved performance for all the indicator/norm pairs, except for the ∞-norm of the actuation at lane B, which is only degraded 2% with respect to the baseline. Nonetheless, the LPV controller provides a reduction on the TVC consumption (the 2-norm of the actuation is reduced 10% at lane A and 5% at lane B). As for the $Q\alpha$ performance, as it was already observed in Figure 7, the maximum peaks of the LPV controller are reduced 22%. The tracking performance is also improved, particularly over the y-axis. Finally, the drift and drift-rate performance are significantly improved as it can be seen at the left-side of Figure 8.

5. CONCLUSION

This paper presents a LPV control design for the VEGA atmospheric-phase control system. The design is performed using VNG, which is the actual VEGA scheduling variable, as a time-varying parameter. In addition, information about its rate variation (non-gravitational acceleration) is also considered in the design process.

A grid-based approach is used to obtain a LPV model of VEGA launcher. The control problem is formulated as a robust control design problem, where the requirements are expressed in terms of weighting functions. The weighting functions are also defined as grid-based LPV models. This allows to cope with the large dynamical system variations and tackle different design strategies at each design grid point. In order to address the bending mode attenuation, the control effort is weighted by a double notch-filter, which results to be very effective providing gain stabilisation for the first and upper bending modes. Finally, note that the design framework is augmented using a LPV wind turbulence Dryden filter to reduce the performance degradation caused by the wind disturbance.

The LPV controller provides satisfactory linear stability margins throughout the flight envelope. Furthermore, the Monte-Carlo simulations exhibit that the LPV controller provides further improved robust performance with respect to the baseline controller. The same conclusion is obtained using four different wind profiles, giving a measure of the wind disturbance rejection capabilities of this design. In this sense, the wind generator $G_w(s, \theta)$ plays an important role, allowing the optimisation to account for real wind levels. Also note that the final implementation of the LPV controller has 23 states, while the baseline controller has 26 states.

It is important to remark that this synthesis approach allows to design the rigid-body controller and the flexible bending filters in one single procedure. This can be used to reduce the tuning and design effort required for each mission. Indeed, this work aim was to highlight the versatility and capabilities of the LPV robust control design methodologies, which are more systematic and offers more analysis and design capabilities with respect to the classical methods.

REFERENCES

Balas, G. (2002). Linear, parameter-varying control and its application to a turbofan engine. *International Journal of Robust and Nonlinear Control*, 12(9), 763–796.

Bedrossian, N., Jang, J., Alaniz, A., Johnson, M., Sebelius, K., and Mesfin, Y. (2005). International space station US GN&C attitute hold controller design for orbiter repair maneuver. In *Proceedings of the AIAA Guidance, Navigation, and Control Conference and Exhibit*.

Brito, A., França, S., and Filho, W.L. (2008). Varying-time notch filter for bending modes active suppression in aerospace systems. In *Proceedings of the 7th International ESA-GNC Conference*.

Ganet, M. and Ducamp, M. (2010). LPV control for flexible launcher. In *AIAA Guidance, Navigation, and Control Conference*. AIAA.

Hjartarson, A., Seiler, P., and Packard, A. (2015). LPVTools: A toolbox for modeling, analysis, and synthesis of parameter varying control systems. *IFAC-PapersOnLine*, 48(26), 139 – 145.

Marcos, A. and Balas, G. (2004). Development of linear-parameter-varying models for aircraft. *Journal of Guidance, Control, and Dynamics*, 27(2), 218–228.

Marcos, A. and Bennani, S. (2009). LPV modeling, analysis and design in space systems: Rationale, objectives and limitations. In *AIAA Guidance, Navigation, and Control Conference*. AIAA.

Marcos, A. and Bennani, S. (2011). *A Linear Parameter Varying Controller for a Re-entry Vehicle Benchmark*, 15–27. Springer Berlin Heidelberg, Berlin, Heidelberg.

Navarro-Tapia, D., Marcos, A., Bennani, S., and Roux, C. (2017). Structured H-infinity and linear parameter varying control design for the VEGA launch vehicle. In *Proceedings of the 7th European Conference for Aeronautics and Aerospace Sciences (EUCASS)*.

Orr, J. (2013). Optimal recursive digital filters for active bending stabilization. In *Proceedings of the AAS Guidance, Navigation, and Control Conference*.

Roux, C. and Cruciani, I. (2008). Scheduling schemes and control law robustness in atmospheric flight of VEGA. In *Proceedings of the International ESA-GNC Conference*.

Simplício, P., Bennani, S., Marcos, A., Roux, C., and Lefort, X. (2016). Structured singular-value analysis of the vega launcher in atmospheric flight. *Journal of Guidance, Control, and Dynamics*, 39(6), 1342 – 1355.